Planetary Nebulae: An Eye to the Future
Proceedings IAU Symposium No. 283, 2011
A. Manchado, L. Stanghellini & D. Schönberner, eds.

doi:10.1017/S1743921312011817

Further exploration of Galactic disk abundance gradients

Jackie B. Milingo[1], Richard B. C. Henry[2], Karen B. Kwitter[3] and Bruce Balick[4]

[1]Department of Physics, Gettysburg College, Gettysburg, PA 17325, USA
email: jmilingo@gettysburg.edu, henry@nhn.ou.edu, kkwitter@williams.edu

[2]Department of Physics & Astronomy, University of Oklahoma, Norman, OK 73019, USA

[3]Department of Astronomy, Williams College, Williamstown, MA 01267, USA

[4]Department of Astronomy, University of Washington, Seattle, WA 98195, USA
email: balick@astro.washington.edu

Abstract. We examine the abundance gradient in the Milky Way disk via homogeneously determined data for 124 Galactic planetary nebulae (PNe). We present recent results from a detailed regression analysis of the O gradient. With O, Ne, S, Cl, and Ar available and a range of galactocentric distance (R_g) from 0.9 to 21 kpc, we present additional exploration of the disk radial gradient by statistically analyzing a series of short segments of increasing average R_g.

Keywords. Galaxy: abundances, Galaxy: evolution, ISM: abundances, planetary nebulae: general

1. Introduction, data and analysis

The breadth in progenitor mass for PNe make them useful probes of both stellar nucleosynthesis and galactic chemical evolution. Abundances from Galactic PNe covering a large range in R_g can be used to map out the spatial and temporal distribution of nuclear species in the disk. Abundance gradients from PNe help constrain our understanding of the chemical and dynamic history of the Galaxy.

This study includes 124 PNe whose progenitors belong to the disk population (Peimbert Types I and II) and extend from ∼1 to 21 kpc in R_g. Linear regression analysis was performed for O, Ne, S, Cl, and Ar accounting for uncertainties in both abundance and radial distance (± 20% in R_g, Stanghellini *et al.* 2006). Uncertainties in 12+log(X/H) were adjusted using a scaling factor $f(X)$ until the fit accounted for all of the scatter in the data. This optimized fit yields $\widetilde{\chi}^2 = 1$ (see Henry *et al.* 2010). Fits and resultant abundance gradients are shown in Table 1.

Considering the behavior of smaller subsets of the data we split the sample into 6 kpc segments with increasing $\langle R_g \rangle$ in 1 kpc steps. For each segment we performed a linear regression analysis using the optimized abundance uncertainties. Figure 1(a) shows results from the 6 kpc segments for O, and (b-f) plot the segment slopes vs. $\langle R_g \rangle$ of each segment for O, Ne, S, Cl, and Ar respectively.

2. Conclusions

Optimized fits yield slopes ranging from ∼ –0.05 to –0.08 dex/kpc. We point out the $f(X)$ values that emerged for Ne, S, Cl, and Ar are unexpectedly large and require further examination.

Table 1. Optimized fits ($y = bx + a$), correlation coefficients, correlation probabilities, number of PNe used, and scaling factors (L to R) for O, Ne, S, Cl, and Ar.

X	$b \pm \sigma_b$ (dex/kpc)	$a \pm \sigma_a$	R	P_R	N	$f(X)$
O	–0.058 ± 0.006	9.09 ± 0.05	–0.53	< 0.00001	124	1.40
Ne	–0.061 ± 0.011	8.54 ± 0.09	–0.31	0.0004	122	2.51
S	–0.083 ± 0.011	7.36 ± 0.08	–0.51	< 0.00001	124	1.94
Cl	–0.086 ± 0.011	5.79 ± 0.08	–0.51	< 0.00001	112	1.78
Ar	–0.054 ± 0.009	6.86 ± 0.08	–0.39	< 0.00001	124	2.61

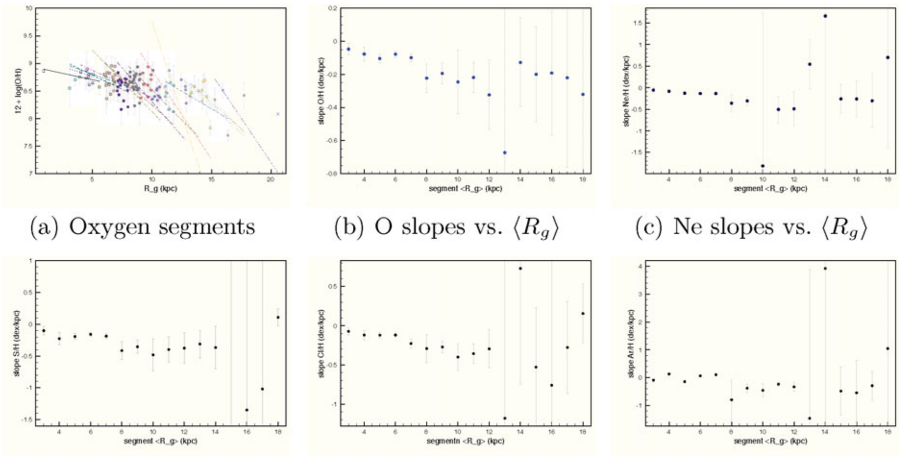

(a) Oxygen segments (b) O slopes vs. $\langle R_g \rangle$ (c) Ne slopes vs. $\langle R_g \rangle$

(d) S slopes vs. $\langle R_g \rangle$ (e) Cl slopes vs. $\langle R_g \rangle$ (f) Ar slopes vs. $\langle R_g \rangle$

Figure 1. Slopes for 6 kpc segments. Error bars (b-f) indicate uncertainties in the fit slopes.

Fit slopes found for the 6 kpc segments, Fig. 1 (b-f), indicate behavior not inconsistent from Twarog *et al.* (1997) who report a discontinuity in [Fe/H] (via open clusters) at 10 kpc due to the history of dynamics in the Galactic disk. Although some of the resulting gradients display unrealistic artifacts from the scatter and uncertainty in the PNe data within each segment, the general trend shows shallow gradients with small error bars at <8–10 kpc, a statistically significant (though more uncertain) steepening of gradients from 8–12 kpc, and highly uncertain gradients beyond 12 kpc.

The paucity of PNe data beyond $R_g \sim 15$ kpc makes the nature of the gradient (linear, steepening, flattening, a step function) uncertain. The spread in abundances at a given R_g and the uncertainties in those abundances, as implied by the optimized linear fits, are indicative of a number of contributions including the uncertainty that emerges from the abundance determination process, true dispersion in PNe abundances due to the breadth in progenitor mass and age, contributions from the underlying abundance gradient (natal metallicity, location in R_g), and dispersion/migration of the PNe progenitor from its birthplace.

References

Henry, R. B. C., Kwitter, K. B., Jaskot, A. E., Balick, B., Morrison, M. A., & Milingo, J. B. 2010, *ApJ*, 724, 748

Stanghellini, L., Guerrero, M. A., Cunha, K., Manchado, A., & Villaver, E. 2006, *ApJ*, 651, 898

Twarog, B. A., Ashman, K. M., & Anthony-Twarog, B. J. 1997, *AJ*, 114, 2556

https://doi.org/10.1017/S1743921312011817 Published online by Cambridge University Press